Injectable muscle-adhesive antioxidant conductive photothermal bioactive nanomatrix for efficiently promoting full-thickness skeletal muscle regeneration

Li Zhou [a,c], Juan Ge [c], Min Wang [c], Mi Chen [c], Wei Cheng [c], Wenchen Ji [f], Bo Lei [b,c,d,e,*]

[a] *Key Laboratory of Special Functional and Smart Polymer Materials of Ministry of Industry and Information Technology, School of Natural and Applied Sciences, Northwestern Polytechnical University, Xi'an, 710129, China*
[b] *Key Laboratory of Shaanxi Province for Craniofacial Precision Medicine Research, College of Stomatology, Xi'an Jiaotong University, Xi'an, 710049, China*
[c] *Frontier Institute of Science and Technology, Xi'an Jiaotong University, Xi'an, 710049, China*
[d] *National and Local Joint Engineering Research Center of Biodiagnosis and Biotherapy, The Second Affiliated Hospital of Xi'an Jiaotong University, Xi'an, 710000, China*
[e] *Instrument Analysis Center, Xi'an Jiaotong University, Xi'an, 710054, China*
[f] *Department of Orthopedics, The First Affiliated Hospital of Xi'an Jiaotong University, 710061, China*

ARTICLE INFO

ABSTRACT

The completed skeletal muscle regeneration resulted from severe injury and muscle-related disease is still a challenge. Here, we developed an injectable muscle-adhesive antioxidant conductive bioactive photothermo-responsive nanomatrix for regulating the myogenic differentiation and promoting the skeletal muscle regeneration *in vivo*. The multifunctional nanomatrix was composed of polypyrrole@polydopamine (PPy@PDA, 342 ± 5.6 nm) nanoparticles-crosslinked Pluronic F-127 (F127)-polycitrate matrix (FPCP). The FPCP nanomatrix demonstrated inherent multifunctional properties including excellent photothermo-responsive and shear-thinning behavior, muscle-adhesive feature, injectable ability, electronic conductivity (0.48 ± 0.03 S/m) and antioxidant activity and photothermal function. The FPCP nanomatrix displayed better photothermal performance with near-infrared irradiation, which could provide the photo-controlled release of protein (91% ± 2.6% of BSA was released after irradiated 3 times). Additionally, FPCP nanomatrix could significantly enhance the cell proliferation and myogenic differentiation of mouse myoblast cells (C2C12) by promoting the expressions of myogenic genes (MyoD and MyoG) and myosin heavy chain (MHC) protein with negligible cytotoxicity. Based on the multifunctional properties, FPCP nanomatrix efficiently promoted the full-thickness skeletal muscle repair and regeneration *in vivo*, through stimulating the angiogenesis and myotube formation. This study firstly indicated the vital role of multifunctional PPy@PDA nanoparticles in regulating myogenic differentiation and skeletal muscle regeneration. This work also suggests that rational design of bioactive matrix with multifunctional feature would greatly enhance the development of regenerative medicine.

1. Introduction

Skeletal muscle, as an important part of the human body, is responsible for controlling voluntary movement and possesses robust regeneration capability after the minor injury with the help of satellite cells [1]. Nonetheless, the regeneration of skeletal muscle is limited owing to the traumatic injury, surgical procedures or neuromuscular disorders [2]. The common clinical strategies for repairing skeletal muscles include the implantation of host muscle and muscle precursor cells or pre-engineered myoblasts to the target site [3]. Although these strategies provided some positive results, the treatment of muscle injury was still not satisfactory because of the significant donor site morbidity, immune rejection, poor delivery and insufficient donor cells [4]. Thus, it is very necessary to develop new strategies to reconstruct the lost or damaged muscles.

At present, various biomaterials-based strategies have been explored

for potential application in repair and regeneration of skeletal muscles [5]. In these strategies, conducting biomaterials including carbon/metal and polymer-based semiconductors have become promising candidates due to their electrical signal transmission ability that could improve the myoblasts proliferation and myogenic differentiation [6–10]. Polypyrrole (PPy) was one of the most studied conducting polymers attributed to its easily preparation, excellent conductivity and biocompatibility [11]. Previous studies showed that PPy-based nanomaterials could enhance the proliferation and myogenic differentiation of myoblasts *in vitro*. However, the application of PPy in tissue engineering was restricted by its bad degradability and solubility and poor mechanical properties [12,13]. Ideally, the exploitation of multifunctional biomaterials with controlled conductivity was highly desirable for *in vivo* application in skeletal muscle regeneration. To resolve these drawbacks, polymer composites originated from PPy and biocompatible polymers such as dopamine [14], chitosan [15], polycaprolactone (PCL) [16], and poly (lactide-co-glycolide) (PLGA) [17] have been developed for tissue engineering. Unfortunately, if PPy could enhance the skeletal muscle regeneration *in vivo* is still not reported.

In addition to the conductive activity, the antioxidative activity also presented the good capacity for enhancing tissue regeneration through decreasing the oxidative stress and reactive oxygen species. The antioxidative bioactive biomaterials have been developed and showed the promising application in regenerative medicine and tissue engineering [18]. Moreover, the injective and adhesive abilities for biomaterials were also important during the surgery and increasing tissue adhesion. Polydopamine (PDA) as a biocompatible adhesive material has been widely used in biomedicine owing to its low toxicity and mussel-inspired characteristic [19–22]. Adhesive hybrid biomaterials could be obtained by the amidation or Schiff-base reaction between the biopolymers and PDA [23]. However, the role of PDA in myogenic differentiation and skeletal muscle regeneration *in vivo* is also not clear. Recently, the biomedical polymers based on citric acid have been developed and attracted much attention, due to their good biocompatibility, biomimetic viscoelasticity and low cost [24,25]. Our group also reported a series of citric acid-based hybrid polymers and demonstrated their promising biomedical applications in bioimaging, drug delivery/obesity therapy and skin regeneration [26–30]. Recent studies exhibited that citric acid-based polymers could efficiently improve the angiogenesis which was the vital step during the tissue formation [31]. Therefore, it was very promising to design citric acid-based biomaterials matrix with multifunctional properties for enhanced skeletal muscle regeneration.

Herein, we designed an injectable multifunctional polypyrrole@polydopamine (PPy@PDA) crosslinked nanocomposite hydrogel, which displays the temperature-responsive gelation property between a liquid and a gel state during temperature transition, with excellent adhesive behavior, antioxidant ability and electrical conductivity for stimulating the myoblast differentiation *in vitro* and skeletal muscle regeneration *in vivo*. The multifunctional hydrogel was obtained by the crosslinking of poly (citrate-glycol)-polyethylenimine (PCE), carboxymethyl chitosan (CMC), dibenzaldehyde-terminated F127 (F127-Phe-CHO) and PPy@PDA nanoparticles (F127-PCE-CMC-PPy@PDA, FPCP). PPy@PDA was used to achieve photothermal effect, antioxidant ability and electronic conductivity. CMC and PCE which could stimulate cell proliferation with low cytotoxicity in our previous report [29], were served as the crosslinked network. F127-Phe-CHO was served as the temperature-sensitive component, which formed the gel network by Schiff-base reaction between its aldehyde group and quinone group on PPy@PDA and amino group of CMC and PCE. It was anticipated that multifunctional FPCP nanomatrix could significantly stimulate the myoblast differentiation *in vitro* and skeletal muscle regeneration *in vivo* [8,32].

2. Methods

2.1. Fabrication and characterizations of FPCP hydrogel

PCE polymer and dibenzaldehyde-terminated F127 (F127-Phe-CHO) were synthesized as described previously [26,30,33]. PPy@PDA was prepared through an oxidative polymerization method as described in Supporting Information. The FPCP hydrogel was obtained by a facile mixing method. In brief, 20 wt% F127-Phe-CHO solution, 50 wt% PCE solution, 15 wt% CMC solution and 5 wt% PPy@PDA aqueous solution were prepared, respectively. Then, 10 μL PPy@PDA solution (0.5 mg, 5 wt%), 20 μL PCE solution (10 mg, 50 wt%) and 200 μL CMC solution (30 mg, 15 wt%) were added into 300 μL F127-Phe-CHO (60 mg, 20 wt%) at ice. The mixture was maintained at 37 °C to form the FPCP hydrogel after mixing. Similarly, the hydrogels without PPy@PDA or PCE and PPy@PDA (instead of H_2O) were fabricated through the same procedure and were designed as controls, denoted as FPC and FC, respectively. The composition of various hydrogels was presented in Table S1.

The Fourier transform infrared spectroscopy (FTIR) of FCHO, CMC, FC, FPC, FPCP hydrogel and FPCP hydrogel after laser irradiation (808 nm, 1.41 W cm^{-2}, 10 min) were measured in the range between 4000 and 400 cm^{-1} (Bruker VERTEX70). The PDA decorated PPy was characterized by UV–vis spectrophotometer (PE Lambda950). The structure of PPy@PDA, FPC and FPCP hydrogel were determined by transmission electron microscopy (TEM, JEOL JEM-F200) at an accelerating voltage of 100 kV. The morphology of FPCP hydrogel and controls were observed by a field emission scanning electron microscope (FE-SEM, Zeiss GeminiSEM 500) after sprayed with gold. The particle size of PPy@PDA dispersion solution and elemental analysis of FPCP hydrogel were tested using dynamic light scattering (DLS) (Zetasizer Nano ZS90, Malvern) and X-ray photoelectron spectroscopy (XPS, Thermo Fisher ESCALAB Xi+), respectively.

2.2. Rheological properties and injectable performance assay

The rheological property of FPCP hydrogel and controls were analyzed using a DHR-2 TA rheometer. Briefly, the storage modulus (G′) and loss modulus (G″) of samples were evaluated under different conditions, containing temperature change of 4–38 °C (1% oscillation strain and 1 Hz frequency), increasing the oscillation strain (0.1%–1000%) and 1%-1000%–1% oscillation strain for three cycles at 37 °C and 1 Hz frequency. Additionally, the viscosity of samples was also determined at different temperature (4–38 °C) and shear rate (0.1–100 s^{-1}). The injectability of the FPCP hydrogel was evaluated by extruded through the 1 mL syringe without clogging as described previously [34].

2.3. Photothermal effect and in vitro drug release study

The photothermal performances of the FPCP hydrogel, FPC, FC, FCHO and H_2O were measured in a 24-well culture plate upon exposure to an 808 nm laser (diameter: ~15 mm, 1.41 W cm^{-2}) for 10 min. FPCP without irradiation was designed as control. The temperature changes and thermal images were tested by an infrared thermal imaging system (Fluke VT04A Visual IR Thermometer) in real time.

BSA was chosen to evaluate the *in vitro* drug release behavior of FPCP hydrogel and FPC at the irradiation of 808 nm laser (1.41 W cm^{-2}). Briefly, 0.5 mL of FPC or FPCP hydrogels loaded with BSA (1 mg) were placed into 0.5 mL H_2O and exposure to an 808 nm laser for 10 min, then shaking with 100 rpm at constant temperature (37 °C) for 30 min, respectively. Then, 0.5 mL of release solution was withdrawn, and 0.5 mL of fresh H_2O was added to keep constant volume. After irradiation-shaking 4 cycles, the concentrations of the BSA released from hydrogels were measured by the UV–vis spectrophotometer (PerkinElmer Lambda 35). The λ_{max} of BSA was 276 nm. Samples without irradiation were used as controls. The BSA cumulative release (%) was calculated by the ratio of the concentrations of cumulative release to the initial concentration of

BSA.

2.4. Adhesive strength, antioxidant efficiency and conductivity evaluations

The adhesive capability of the hydrogels to the host tissue was evaluated using fresh mouse skeletal muscle. Briefly, the skeletal muscle was obtained from the BALB/c female mice (25–30 g in weight). 50 μL of FPCP hydrogel solutions (stained with crystal violet) were applied onto the surface of skeletal muscle and another muscle was put onto the hydrogel solution. Subsequently, the muscles were pressed with tweezers for 1 min. The adhesion properties were tested by the macroscopic adhesive experiments through pulling the muscle with the tweezers. The adhesion strength of FPCP hydrogel and controls to fresh porcine skin was determined by a TA rheometer as shown in Supporting Information.

The antioxidant activities of hydrogels were evaluated by determining their capacity to scavenge the DPPH free radical with some modifications [35]. Briefly, the 1 mg lyophilized samples were dissolved in 1 mL H_2O, then was added to the DPPH solution of water and methanol ($V_{water}/V_{methanol}$ = 1:2, 3.0 mL, 100 μM) and incubated in a dark place for 15 min after stirring. Then, the absorbance of the mixture was determined at 517 nm using a UV–vis spectrophotometer. The DPPH degradation was calculated by the following equation:

$$DPPH\ scavenged\ \% = \frac{A_B - A_S}{A_B} \times 100\%$$

where A_B is the absorption of the blank (DPPH + H_2O + methanol), A_S is the absorption of the sample (DPPH + H_2O + methanol + sample).

The conductivity of the hydrogels was measured according to the previous report [36]. Briefly, 100 μL hydrogels were prepared on the coverslips, and then the sheet resistance (R_S) and thickness (t) of samples were determined by a digital four-probe tester with a linear probe head (1.0 mm space, 1 mA, Agilent Model B2900A) and dial indicator, respectively. The conductivity (σ) was calculated by the following equation:

$$\sigma = \frac{1}{R_s t}$$

2.5. Cytotoxicity and myogenic differentiation analysis

The cytotoxicity of FPCP hydrogel was evaluated by the alamarBlue® assay (Molecular Probes) and LIVE/DEAD kit (Invitrogen) in C2C12 cells. The cell morphology of stained C2C12 was imaged by fluorescence microscope (Leica TCS SP8 STED 3X). The *in vivo* toxicity of PPy@PDA nanoparticles was evaluated using the blood test and histology analysis of major organs of mouse at 1, 3 and 7 day after intraperitoneal injection of PPy@PDA (Supporting Information). The effect of FPCP hydrogel on the myogenic differentiation of C2C12 cells was determined by analyzing the formation of myotube and myogenic genes expressions (myogenin (MyoG), myogenic differentiation antigen (MyoD), the myosin heavy chain (MHC) protein, Supporting Information).

2.6. Animal experiment of full-thickness skeletal muscle defect

The effect of FPCP hydrogel on skeletal muscle regeneration was measured by a rat tibialis anterior muscle defect model as previously reported [6,8]. The animal experiments were performed by the Guideline for the laboratory animals with the approval of the animal ethics committee of Xi'an Jiaotong University. In brief, the tibialis anterior muscle of SD rats (female, 180 g–200 g, n = 6) was exposed by incised the anterolateral skin after anesthetized with chloral hydrate. The rat tibialis anterior muscle defect model was obtained by created a cuboid-shaped defect (5 mm × 3 mm × 2 mm, the mass of the removed defect was about 10 mg) on the muscle belly. Then, the muscle defects

were filled with FPCP hydrogel (50 μL), FPC and FC, respectively. The group without any filler was used as control. Finally, the absorbable surgical suture was used to suture the skin incision. At predesigned time intervals (1 week and 4 weeks), rats were sacrificed and the tibialis anterior muscles were harvested and photographed. The muscles were then fixed in 10% (v/v) formaldehyde solution, embedded in paraffin and sectioned. Hematoxylin and eosin (H&E) staining, CD31 immunofluorescence staining, Masson's trichrome staining and IL-6 staining of tissue sections were performed for evaluating the repair, capillary density, regeneration and inflammation of tissue in the defect area, respectively. The myofiber diameter and the number of centronucleated myofiber in skeletal muscle defect were measured by analyzing the H&E images. Three randomly selected fields of each section and three sections per specimen were observed with a light microscope (BX53, Olympus, Japan), and the digitized information was analyzed by ImageJ software.

2.7. Statistical analysis

All data were expressed as mean ± standard deviation (n = 3). Statistically significant value was set as $p < 0.05$ using student's T –test (two tails, unequal variance) and analysis of variance.

3. Results and discussion

3.1. Preparation and characterization of FPCP hydrogel

The F127-Phe-CHO and PCE were synthesized according to the routine shown in Fig. 1A [37]. PPy@PDA NPs were prepared by chemical oxidation and then decorated with a mussel-inspired PDA layer from the polymerization of DA [38] (Fig. 1B). The FPCP hydrogel network was formed by Schiff-base reaction between the $-NH_2$ of PCE/CMC and the –CHO of F127-Phe-CHO and PPy@PDA, respectively (Fig. 1C). It was expected that FPCP hydrogel possess the multifunctional features including injectability/adhesiveness/antioxidation/conductivity, and could significantly promote skeletal muscle regeneration *in vivo*. The chemical structures of PCE, F127-Phe-CHO, CMC, FC, FPC, FPCP and FPCP with or without NIR irradiation were analyzed by FTIR (Fig. 2A and Figs. S1A–B). The absorption of ester bonds (–C(O)–) and –NH– stretching band of PCE polymer appeared at 1736 cm^{-1} and 3435 cm^{-1}, respectively. The absorptions bands at 2873 cm^{-1}, 1687 cm^{-1}, 1603 cm^{-1} and 1099 cm^{-1} were the C–H stretching vibration band, symmetric vibration of carbonyl in aldehyde group, characteristic peak of benzene ring and ether bonds ($-OCH_2CH_2-$) from F127-Phe-CHO, revealing the formation of F127-Phe-CHO. The absorption of amide bond from CMC was observed at 1553 cm^{-1}. As shown in the results of the FC, FPC and FPCP hydrogel, the peak of the imine stretching vibration (C=N) at 1647 cm^{-1} was assigned to the newly formed Schiff-base from amine group of PCE and CMC and aldehyde group of F127-Phe-CHO, demonstrating that the hydrogel network was formed successfully. The almost disappearance of signal at 1687 cm^{-1} in the hydrogels also indicated that –CHO in F127-Phe-CHO was consumed, further indicating that the FPCP hydrogel were successfully prepared by Schiff-base reaction. After irradiation with 808 nm laser (1.41 W cm^{-2}, 10 min), the intensity of C=O stretching vibration at 1736 cm^{-1} of PCE in FPCP hydrogel was decreased and the intensity of C=N stretching vibration at 1647 cm^{-1} was increased, showing that more imine was formed in FPCP hydrogel (Figs. S1A–B).

The PPy@PDA NPs were synthesized (Supporting Information) and measured by UV–vis spectrophotometer and TEM analysis. The absorption peak at ~411 nm was assigned to the PDA and the significant near-infrared absorption between 800 and 1000 nm of PPy@PDA revealed its potential photothermal property [39] (Fig. 2B). The TEM image of PPy-F127 NPs showed their spherical morphology with the size of 50 ± 3.4 nm (Fig. 2C). By comparison, after surface modification, PPy-F127 NPs were coated by a PDA layer with a thickness of 20 ± 2.1 nm, resulting in the PPy@PDA particles (Fig. 2C). Additionally, FPCP
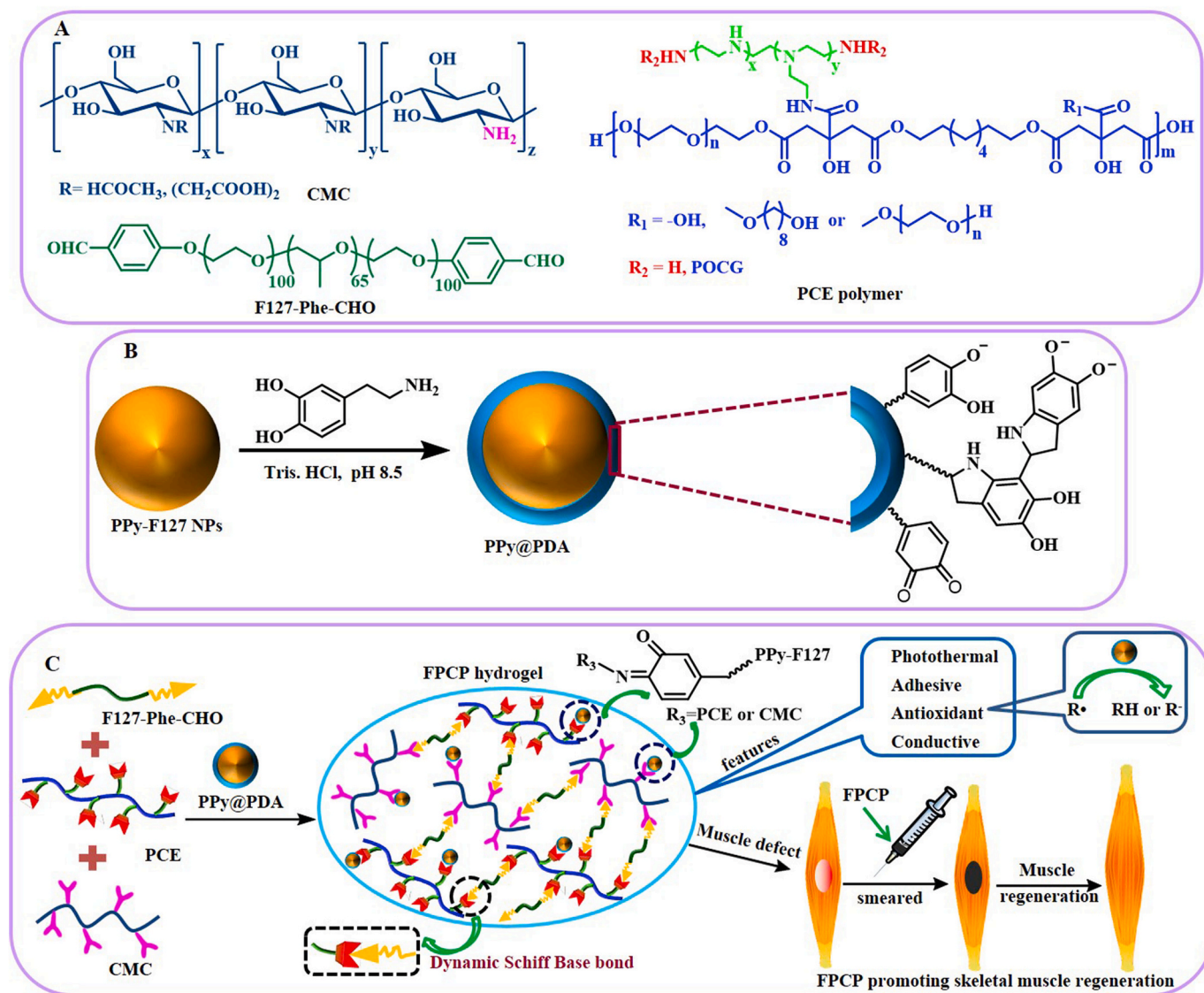
Fig. 1. Scheme showing the preparation and application of multifunctional FPCP hydrogel in skeletal muscle regeneration. (A) Structure of CMC, F127-Phe-CHO and PCE polymer; (B) Synthesis route of PPy@PDA; (C) Schematic illustration for the formation of multifunctional FPCP hydrogel and the application in skeletal muscle regeneration.

hydrogel displayed core-shell structure after incorporating PPy@PDA into FPC hydrogel network, suggesting that the PDA layer of PPy@PDA also participated in the Schiff-base reaction with the –NH₂ of PCE and CMC (Fig. 2C, Fig. S1C and Fig. 1C). The morphologies of FPCP hydrogel and others were analyzed using SEM after freeze-drying. FPCP hydrogels showed interconnected porous structures. Additionally, the DLS size of PPy@PDA in FPCP hydrogel solution was 342 ± 5.6 nm, which was smaller than that of PPy@PDA particles in water (1432 ± 11.3 nm) (Fig. S1D). The XPS result displayed that the relative content of C, N and O elements in FPCP hydrogel were 73.68%, 0.9% and 25.42%, respectively (Fig. S1E).

3.2. Rheological, viscosity and injectable properties

The storage modulus (G′) values of FPCP, FPC and FC were greater than the loss moduli (G″) when the temperature was above 30 °C, suggesting that the successful preparation of hydrogels (Fig. 3A and Fig. S2A). Additionally, the viscosity of FPCP, FPC and FC was higher than FCHO, further confirming the information of hydrogel network (Fig. 3B and Fig. S2A). FPCP was solution state at 25 °C (G″ > G′), then it

became to gel state when the temperature reached 37 °C (G′ > G″), demonstrating the temperature-responsive gelation feature of FPCP hydrogel (Fig. 3A and G). Additionally, the G′, G″ and viscosity of FPCP were higher than that of FPC at 37 °C, suggesting that PPy@PDA participated in FPCP hydrogel network through the reaction of PDA and amine group of PCE or CMC as displayed in Fig. 1. Moreover, FPCP displayed higher viscosity than FPC with the prolonging of incubation times over 15 min at 37 °C, further indicating the contribution of PPy@PDA in the formation of FPCP hydrogel networks (Fig. 3C).

The shear-thinning behavior and rheological recovery of the hydrogels was further evaluated. The intersection point between G′ and G″ of FPCP was 57%, indicating the collapse of the FPCP hydrogel network at this point (Fig. S2C). In addition, the intersection point of FPCP was higher than that of FPC (55%) and FC (24%) attributed to the contribution of PPy@PDA in the networks (Figs. S2C–F). Then, the rheological recovery behavior of the hydrogel was measured by the continuous step strain method. The G′ of FPCP was sharply reduced and G″ > G′ at the high dynamic strain (1000%), demonstrating that the hydrogel network was collapsed (Fig. 3D). When the shear strain switched to 1%, the initial G′ value of hydrogels was returned quickly, even after three
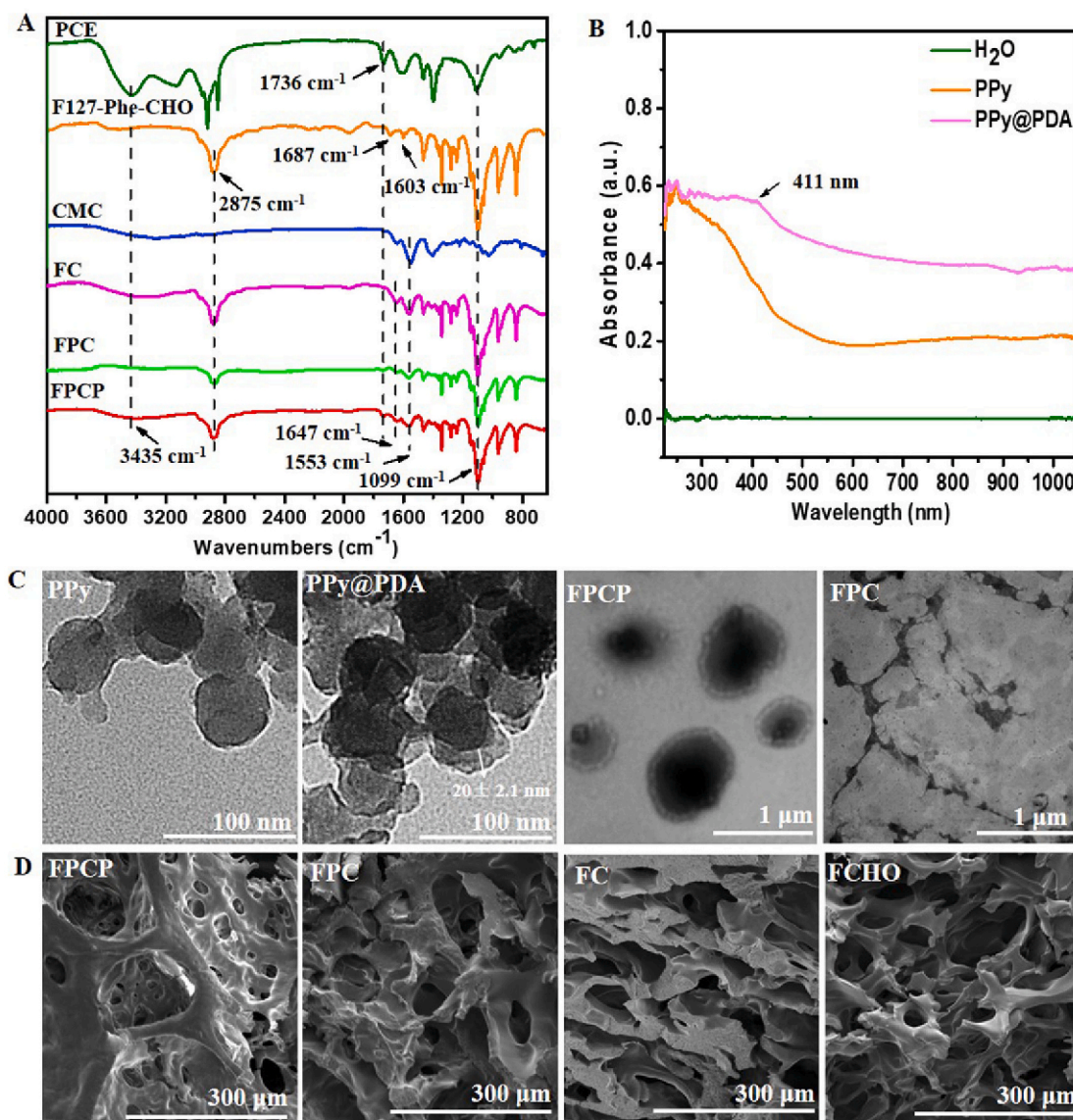
Fig. 2. Physicochemical structure characterizations. (A) FTIR analysis of precursors and FPCP hydrogel; (B) UV–vis spectra of PPy@PDA; (C) TEM images of PPy, PPy@PDA, FPC and FPCP hydrogel; (D) SEM images of FPCP hydrogel, FPC, FC and FCHO.

cycles, indicating the hydrogel network recovered efficiently and rapid shear-thinning property (Fig. 3D and E). Additionally, due to the decrease of FPCP's viscosity with the enhancing of shear rate (Fig. 3F), it could be extruded through the syringe (1 mL) and writing smoothly, demonstrating the good injectability of FPCP (Fig. 3H).

3.3. Photothermal properties and photo-controlled drug release

The thermal images and temperature changes of the FPCP hydrogel and others upon NIR irradiation (808 nm, 1.41 W cm^{-2}) were recorded to evaluate their photothermal performance. The temperature changes (Δ_t) of FPCP hydrogel was rapidly increased and reached 18.5 °C with 10 min irradiation (Fig. 4A and B) because of the contribution of PPy@PDA. By comparison, the Δ_t of FPC, FC and FCHO were slightly higher than that of H$_2$O, suggesting no significant heating effect under the NIR irradiation. No obvious differences in temperature and thermal image of FPCP-NIR group were observed. The photosensitive properties of the FPCP hydrogel could be used for photothermal therapy or photothermal antibacterial applications *in vivo* [40–44].

The photo-controlled drug release behavior of FPCP hydrogel was determined using BSA as a model at the irradiation of laser (808 nm,

1.41 W cm^{-2}). The BSA release rate in FPCP hydrogel accelerated with the times of irradiation, in which 91% ± 2.6% of BSA was detected after irradiated 3 times (Fig. 4C). By comparison, only 54% ± 2.6% of BSA was detected in FPC group even after 4 cycles of irradiation shaking, suggesting the good photo-controlled protein release of FPCP. After shaking for 2 h at 37 °C, approximately 38% ± 5.4% and 39% ± 3.5% of BSA were released in the FPCP-NIR- and FPC-NIR-group (without NIR irradiation), respectively. These results demonstrated that FPCP hydrogel could efficiently release protein drug under the control of NIR irradiation. Additionally, the property of photo-controlled protein release of FPCP suggested that other growth factors, stem cells, genes or drugs could also be photo-controlled release in the FPCP hydrogel. This release manner might be beneficial for the prolonged bioactive molecular accumulation at the defected site and on-demand precise treatment of skeletal muscle regeneration.

3.4. Adhesive, antioxidant and electrical conductivity properties

To promote the skeletal muscle regeneration, the adhesive ability with muscles of FPCP hydrogel was very important for its performance on defect site. The adhesive property of the FPCP hydrogel was
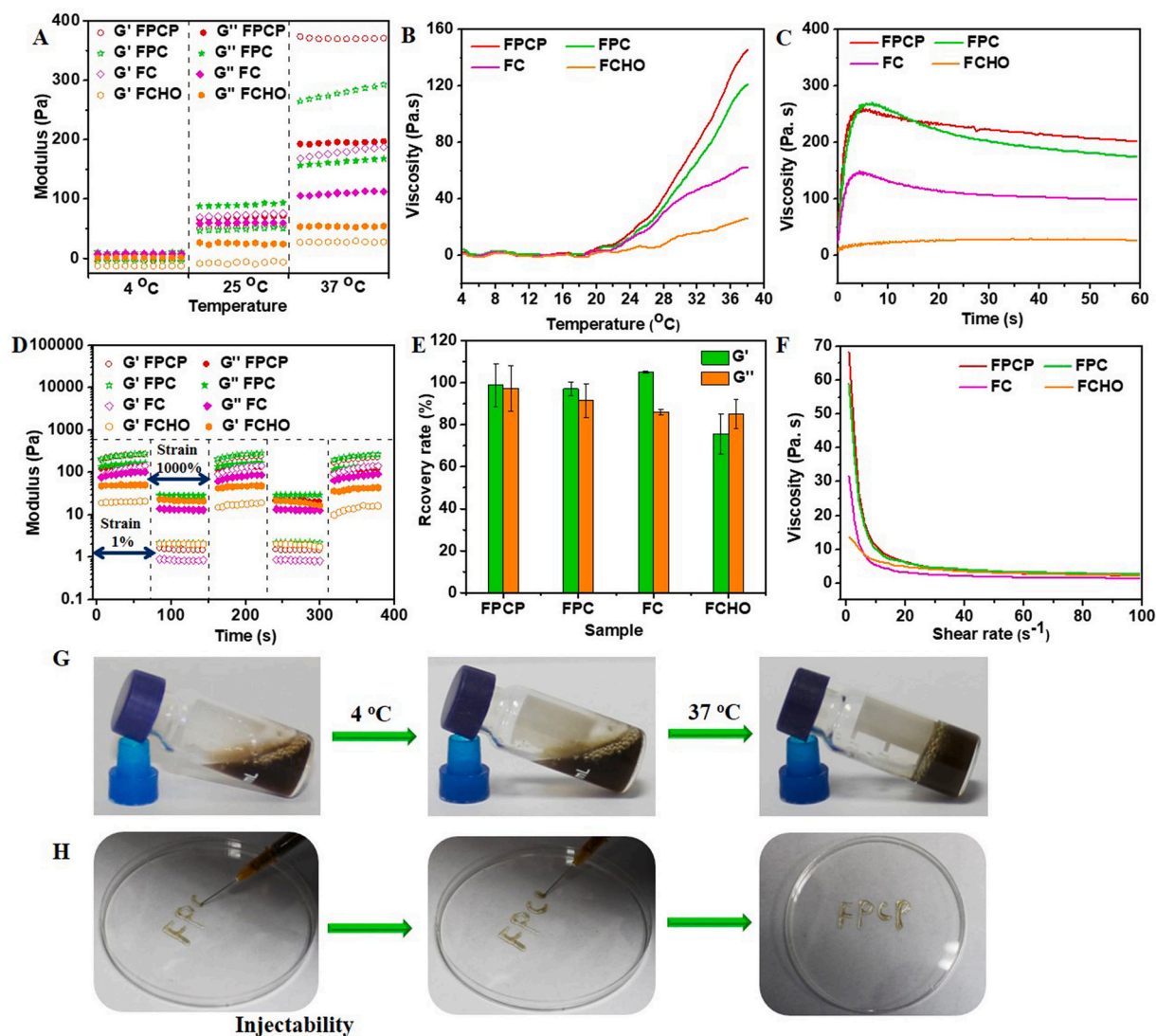
Fig. 3. Rheological properties evaluations. (A) Rheological behavior of the FPCP hydrogel and controls at 4 °C, 25 °C and 37 °C; (B–C) Viscosity of FPCP hydrogel (B) and controls (C) at different temperature and times, respectively; (D) Rheological modulus of samples under alternating high (1000%) and low shear (1%); (E) Rheological recovery rate of samples after high and low shear (n = 3); (F) the viscosity of FPCP hydrogel and controls at different shear rate; (G) Images of the formation of FPCP hydrogel; (H) Photos of injectability of the FPCP hydrogel.

measured through employing a macroscopic pulling testing and quantitative analyzing by a TA rheometer (Fig. 4D and Fig. S3A). The two pieces of skeletal muscles could be adhered closely by FPCP hydrogel (Fig. 4Da and Fig. 4Db), and they were difficult to be separated, suggesting their high adhesive behavior with skeletal muscle (Fig. 4Dc-f). In addition, FPCP hydrogel showed significantly higher adhesive strength to fresh porcine skin than controls (Fig. S3A). These results showed that FPCP displayed desirable adhesive strength which was probably because of the mussel-inspired property of PDA [45]. Additionally, the –CHO of F127-Phe-CHO in the FPCP hydrogel could also interact with –NH$_2$ of cell adhesion molecules and lipids from the surrounding tissue surface by Schiff-base reaction, which was also contributed to the desirable adhesive property of FPCP hydrogel [46].

It was shown that the free radicals existed in the injury site would lead to oxidative stress inhibiting the tissue regeneration [47]. PPy displayed excellent antioxidant activity to scavenge free radicals due to its redox active nature [48]. Herein, the antioxidant capability of FPCP hydrogel was analyzed by determining the scavenging efficiency for DPPH•. The intensity of DPPH• absorption band after adding FPCP hydrogel significantly decreased compared with controls (Fig. S3B). The DPPH• scavenging efficiency in FPCP group was about 32.3% ± 2.3%,

which was significantly higher than that of FPC, FC and FCHO, indicating that FPCP had good antioxidant activity (Fig. 4E).

Skeletal muscle is sensitive to electrical stimulation, which could increase the energy storage in myofibers, induce the myoblasts proliferation and myogenic differentiation. Thus, conducting biomaterials that could build the cellular communication network by enhancing the electrical transmission, have become a promising action for skeletal muscle regeneration [10]. The electrical conductivity of FPCP hydrogel was determined using a four-point probe method [36]. As deposited in Fig. 4F, the conductivity of FPC was about 0.336 ± 0.03 S/m, which was significantly higher than that of FC (0.15 ± 0.02 S/m) due to more amine groups from PCE polymer in FPC. For FPCP hydrogel, the conductivity (0.48 ± 0.03 S/m) was further strengthened by the addition of PPy@PDA owing to the excellent electrical conductivity of PPy (Fig. 4F). FPCP hydrogel displayed a promising potential as muscle regeneration materials because of its better adhesive property, antioxidant ability and higher conductivity.

3.5. Cytotoxicity evaluation

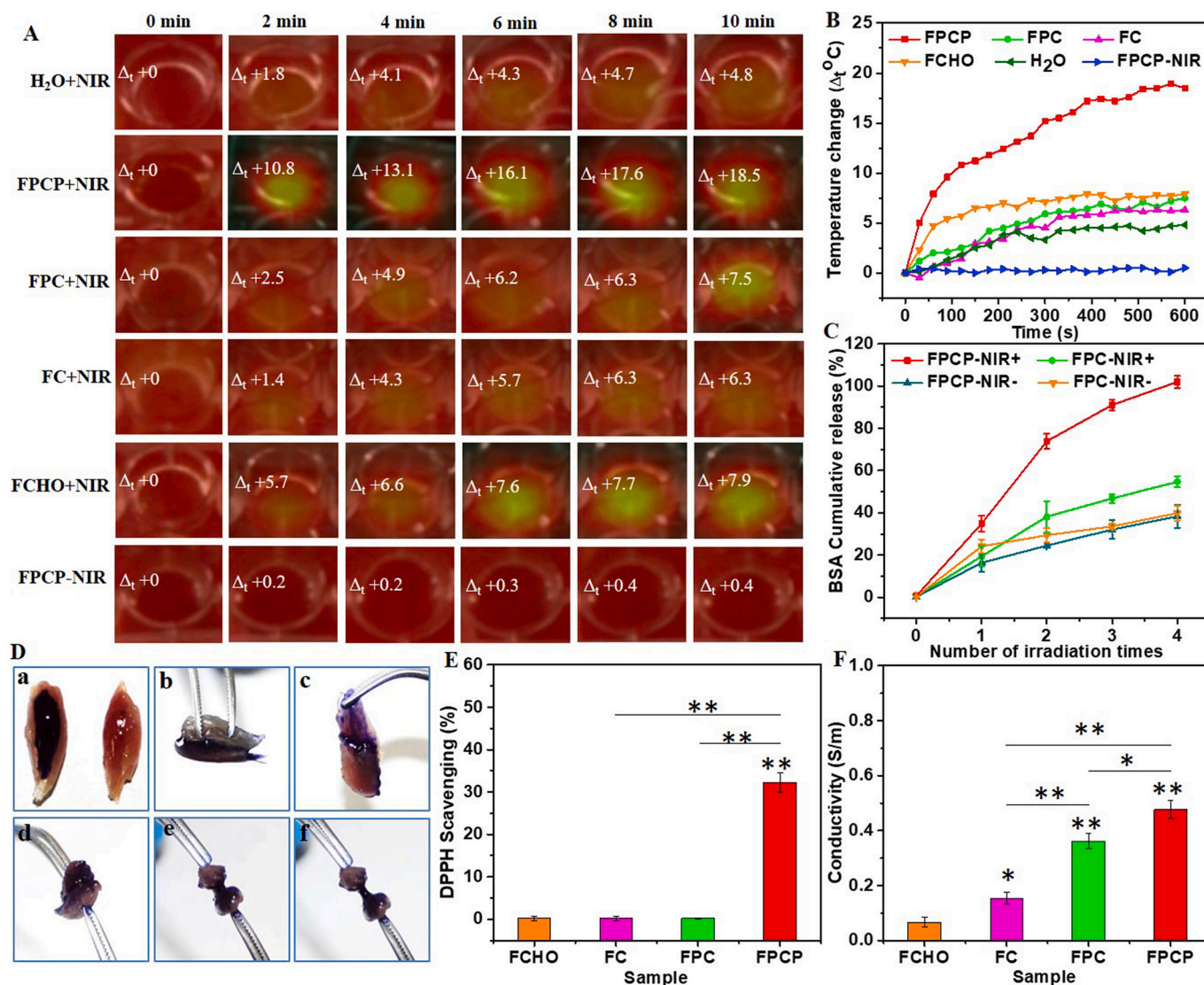The cytotoxicity of FPCP hydrogel was evaluated in C2C12 cells

Fig. 4. Multifunctional properties analysis. (A–B) Real-time infrared thermal images and photothermal heating curves of FPCP hydrogel and controls with NIR irradiation (808 nm, 1.41 W cm^{-2}); (C) NIR-responsive BSA release behavior (BSA cumulative release %) of FPCP hydrogel and controls with or without NIR treatment under four times irradiation (808 nm, 1.41 W cm^{-2}, 10 min/time, n = 3); (D) Images of adhesive test of FPCP hydrogel on skeletal muscle (a: FPCP-coated skeletal muscle, b: pressed muscle, c: adhered muscle, d–f: muscle drawing test); (E) DPPH scavenging percentage by FPCP hydrogel and controls (antioxidant activity) (*$p < 0.05$, **$p < 0.01$, n = 3); (E) Electronic conductivity of FPCP hydrogel and controls (*$p < 0.05$, **$p < 0.01$, n = 3).

under different concentrations (20–100 μg/mL). The image of LIVE/DEAD stained cells displayed that many live cells (green) were observed after incubated with FPCP hydrogel or controls for 1 day (Fig. 5A). After 3 and 7 days, the number of green live cells in all groups dramatically expanded, suggesting the rapid proliferation (Fig. 5A). The cell viabilities of FPCP at day 1 and other controls were greater than 90% even at 100 μg/mL, indicating the low cytotoxicity (Fig. 5B). Additionally, the cell viabilities of FPCP was comparable with that of FPC (without NPs) at the same concentration, suggesting the negligible toxicity of PPy@PDA in C2C12 cells. The cell viability during 7 days was measured to further analyze the relative cell proliferation of FPCP hydrogel and others. No dramatically difference of cell viability among various groups was observed on day 1 (Fig. 5C). After incubation for 3 and 7 days, the relative cell proliferation of all groups were higher than that of 1 day, further indicating their fast proliferation. Moreover, at day 7, FPCP group showed significantly higher relative cell proliferation than others, suggesting that FPCP hydrogel could promote C2C12 myoblast proliferation with the synergy of PPy@PDA owing to its excellent electrical conductivity, which might increase the energy storage in myofibers and

induce cell proliferation, and might have important effect on the myogenic differentiation. Besides, there was no apparent histological changes displayed in liver, heart, spleen, lung and kidney tissues (Fig. S4A), suggesting the minimal organ toxicity from the PPy@PDA. The levels of white blood cell (WBC), lymphocyte (Lymph), monocyte (Mon), red blood cell (RBC), platelet distribution width platelets (PDW) and hemoglobin (HGB) maintained in the normal ranges (Figs. S4B–G) after injection 1, 3 and 7 days, suggesting there was no acute and chronic toxicity of the PPy@PDA. These results indicated the good cytocompatibility of FPCP hydrogel [49,50].

3.6. Myogenic differentiation analysis

The multifunctional physicochemical properties and cell proliferation activity encouraged us to investigate the myogenic differentiation ability of FPCP hydrogel. The immunofluorescent staining of myosin heavy chain (MHC, slow skeletal myosin heavy chain) protein was used to evaluate the myotubes formation and myogenic differentiation in C2C12 cells. The myotube formation could be seen in various groups
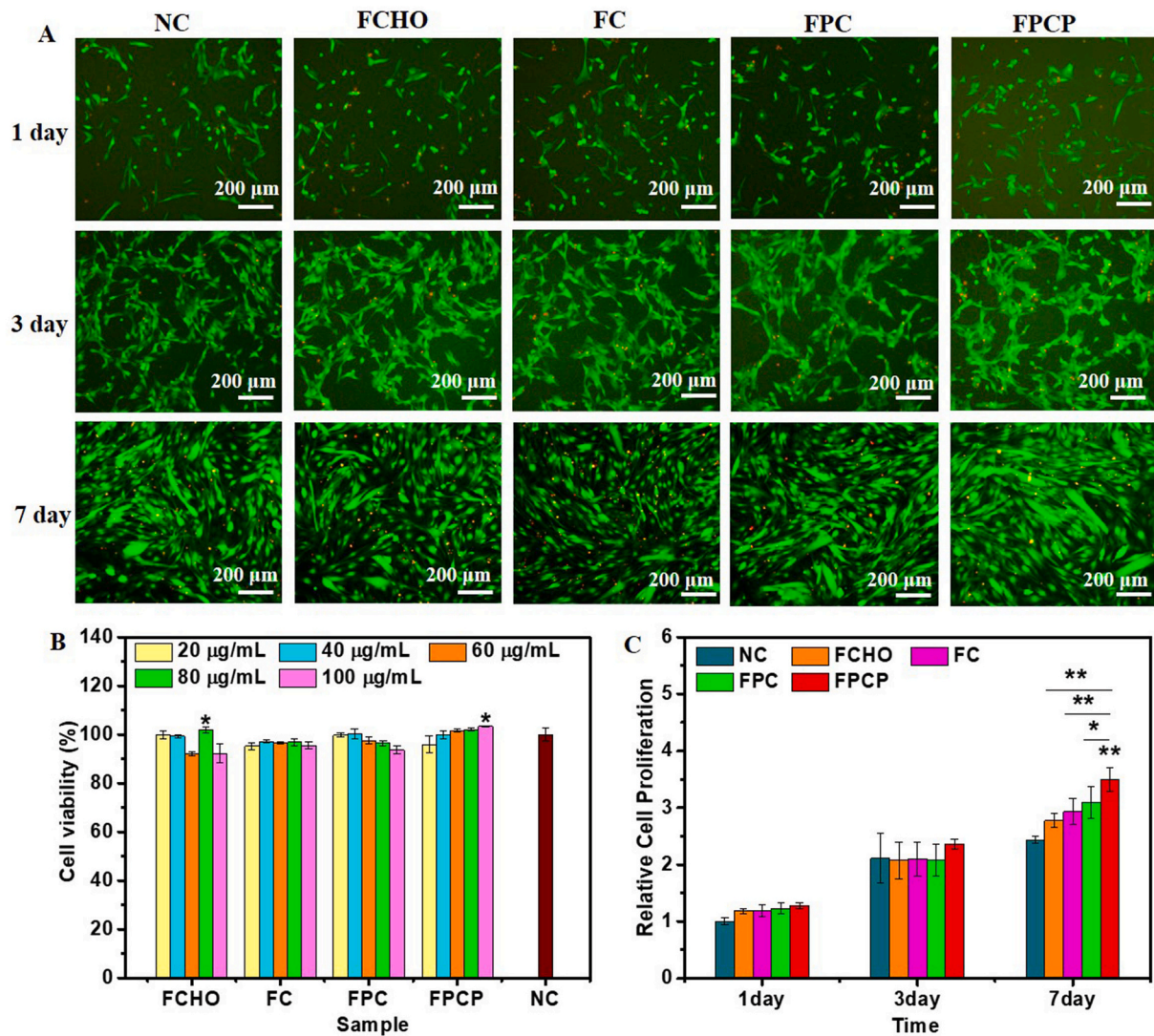
Fig. 5. Cytotoxicity investigations. (A) LIVE/DEAD staining images of C2C12 cells on day 1, 3 and 7 after treated with FPCP hydrogel and controls (80 μg/mL) (live cells: green, dead cells: red, scale bar: 200 μm, n = 3); (B) Cell viability of FPCP hydrogel and each composite in C2C12 cells; (C) Relative proliferation of C2C12 cells treatment with FPCP hydrogel and controls for 1, 3 and 7 days; The relative cell proliferation of 1 day was normalized to that of NC group; The relative cell proliferation on 3 and 7 day was normalized to that of cells cultured for 1 day ($*p < 0.05$, $**p < 0.01$, n = 5). Cells without any treatment was used as negative control (NC).

after 7 days incubation (Fig. 6A and Fig. S5A). Specially, FPCP group showed more myotube numbers than others (Fig. 6A and B). Additionally, FPCP group displayed slightly higher myotube diameter and myotube length than NC group (Fig. 6C). There were no great changes about diameter and length of myotube in FCHO, FC and FPC groups (Fig. 6C and D). FPCP group also showed the significantly high fusion index by comparison with controls (Fig. 6E). Moreover, the expression levels of slow-twitch fiber-associated gene MHC IIa in FPCP group at both gene and protein were obviously higher than that in other groups, suggesting the higher myogenic differentiation ability of FPCP (Figs. S5B–D).

We further analyzed the effect of FPCP on the expressions of myogenic genes MyoD and MyoG in C2C12 cells (Figs. S5E–G). After incubation for 1 day, the gene expression levels of MyoD in FPCP, FPC, FC and FCHO groups were lower than that in NC group. FPCP group showed slightly higher mRNA level of MyoG than that in NC group (Fig. S5E). After culture for 3 days, the highest mRNA levels of MyoD and MyoG was observed in FPCP group. By comparison with NC group, FPC, FC and FCHO groups both increased the gene expression of MyoD and MyoG (Fig. S5F). After culture for 7 days, the mRNA levels of MyoD

and MyoG in FPCP group were further enhanced and exhibited the highest gene expression in all groups (Fig. S5G). These results displayed that FPCP hydrogel probably stimulated the myogenic differentiation of C2C12 myoblasts through up-regulating the expressions of the myogenic genes MyoD and MyoG. The possible mechanism was that PCE as the key component of FPCP hydrogel could enhance the myoblasts proliferation by probably strengthening the mitochondrial number, and could stimulate myogenic differentiation by activating the p38 MAPK γ signaling pathway, which has been approved by our previous study [51]. Additionally, FPCP could build the cellular communication network by enhancing the electrical transmission owing to its excellent electrical conductivity originated from the PPy@PDA, thereby could increase the energy storage in myofibers, induce the myoblasts proliferation and myogenic differentiation [10]. Moreover, the antioxidant activity of FPCP hydrogel could reduce cell damage and promote cell activity through decreasing the oxidative stress and reactive oxygen species [18].
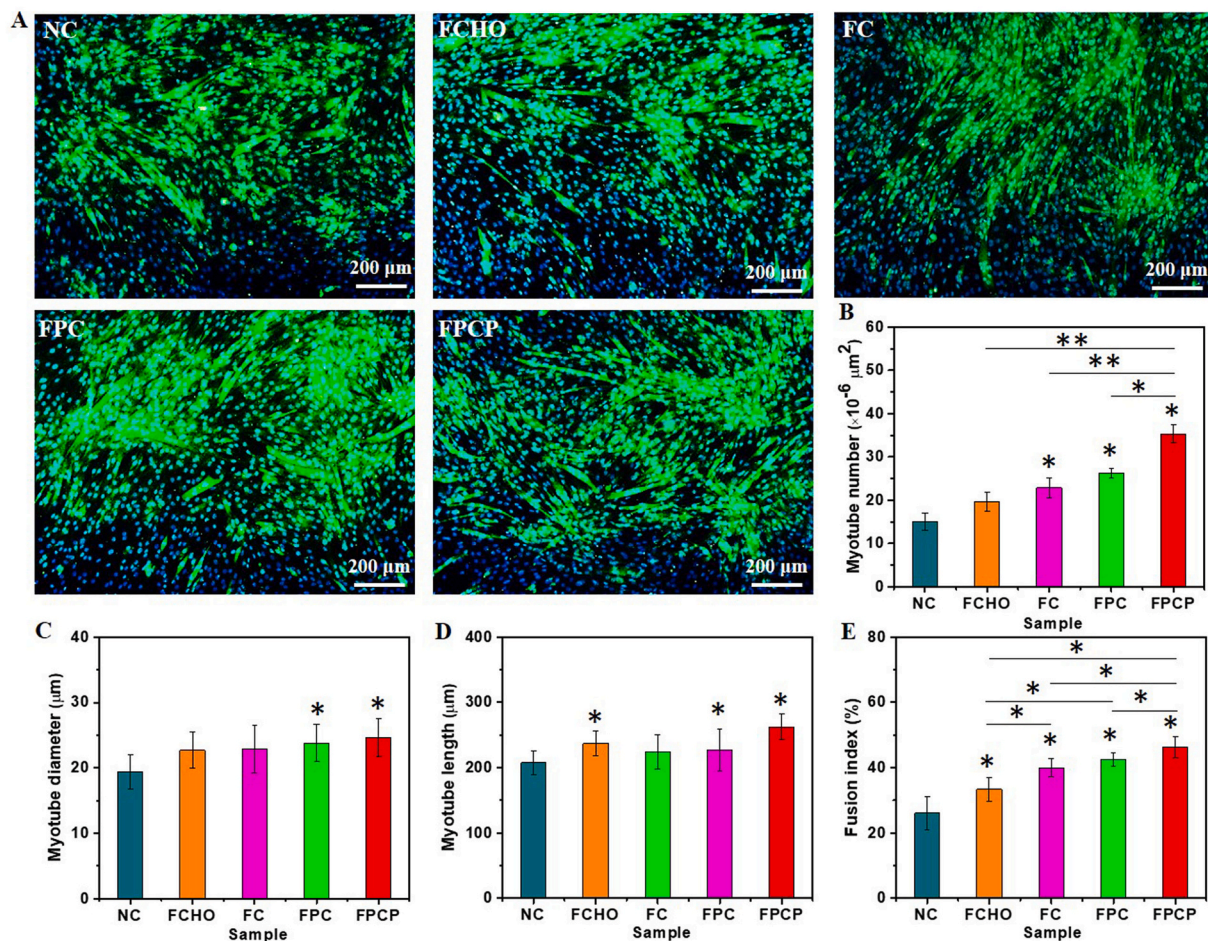
Fig. 6. Myogenic differentiation analysis of C2C12 myoblasts regulated by hydrogels. (A) Immunofluorescence staining of MHC protein in C2C12 after treated with FPCP hydrogel and controls for 7 days, the NC group without hydrogel was used as a control, myotubes and nuclei were stained as green and blue, respectively (scale bar: 200 μm, n = 3); (B–E) Myotube number (B), myotube diameter (C), myotube length (D) and fusion index (E) calculated according to at least three immunofluorescence images of each sample using Image J software (*$p < 0.05$, **$p < 0.01$).

3.7. Skeletal muscle tissue regeneration in vivo

The skeletal muscle regeneration ability of FPCP hydrogel *in vivo* was assessed using a rat tibialis anterior muscle defect as the model. The skeletal muscle regeneration was evaluated by macroscopic observation and histological analysis after surgery for 1 and 4 weeks. After 1 week, some new tissue could be observed in the muscle defect in FPCP and FPC group (Fig. 7A). The blank group and FC group still retained obvious defect (Fig. 7A). The neonatal myofibers are the myofibers of the nucleus at the center of the cytoplasm [52], which could indicate the newly formed skeletal tissue. Here, FPCP group showed more centronucleated myofibers than FPC group attributed to the incorporation of PPy@PDA in the FPCP hydrogel network (Fig. 7B, Fig. S6A). Additionally, FPCP group displayed the strongest fluorescence intensity of CD31 (red) than others, demonstrating the higher capillary density of FPCP group (Fig. 7C–D, Fig. S6B). The diameter of myofibers and number of centronucleated myofibers were also analyzed according to the H&E tissue sections. No significant differences were found in the myofibers diameter in all groups (Fig. 7E). By comparison with other three groups, the FPCP group demonstrated the more centronucleated myofibers numbers, suggesting that more newborn myofibers were formed in FPCP group [6] (Fig. 7F). The image of Masson's trichrome staining demonstrated the reduction of connective tissue in the FPCP treated animals (Fig. S7A). The collagen volume fraction of FPCP was higher than that of others, indicating the more collagen deposition of FPCP group (Fig. S7C). Additionally, the inflammation occurred in FPCP group was

lower than controls (Blank, FC, FPC) as shown in the image of IL-6 staining (red) (Figs. S7B and S7D).

After 4 weeks, the skeletal muscle defect in FPCP group was almost completely repaired and appeared a smooth surface. Other groups (Blank, FC, FPC) also displayed some new tissue in the lacerated regions, although some obvious defect still existed, especially in blank and FC groups (Fig. 8A). According to the H&E images, the skeletal muscle defect in FPCP group was almost filled by new tissue, more centronucleated myofibers could be found in FPCP group by comparison with others (Fig. 8B, Fig. S8A). Additionally, the fluorescence intensity of CD 31 in FPCP group was obviously greater than that of others (Fig. 8C and D). No significant difference in myofibers diameter for various groups (Fig. 8E). The quantitative statistic indicated that the centronucleated myofibers number in FPCP group was much higher than that in other groups (Fig. 8F). Additionally, as shown in Fig. S9A, the collagen fibers (blue) and muscle fibers (red) could be obviously observed in all groups, suggesting that there was regenerated muscle tissue in all injured area. Additionally, the collagen volume fraction of FPCP group was higher than that in FC and NC groups, which was lower than that in FPC group (Fig. S9C). The image of IL-6 staining displayed that the inflammation in FPCP groups was lower than that in other groups (Blank, FC, FPC) (Figs. S9B and S9D). These results suggested that FPCP hydrogel could efficiently accelerate the skeletal muscle regeneration *in vivo* through reinforcing the formation of myofibers and decreasing the inflammation. The probable reason was that FPCP hydrogel had better adhesive property and antioxidant ability, which
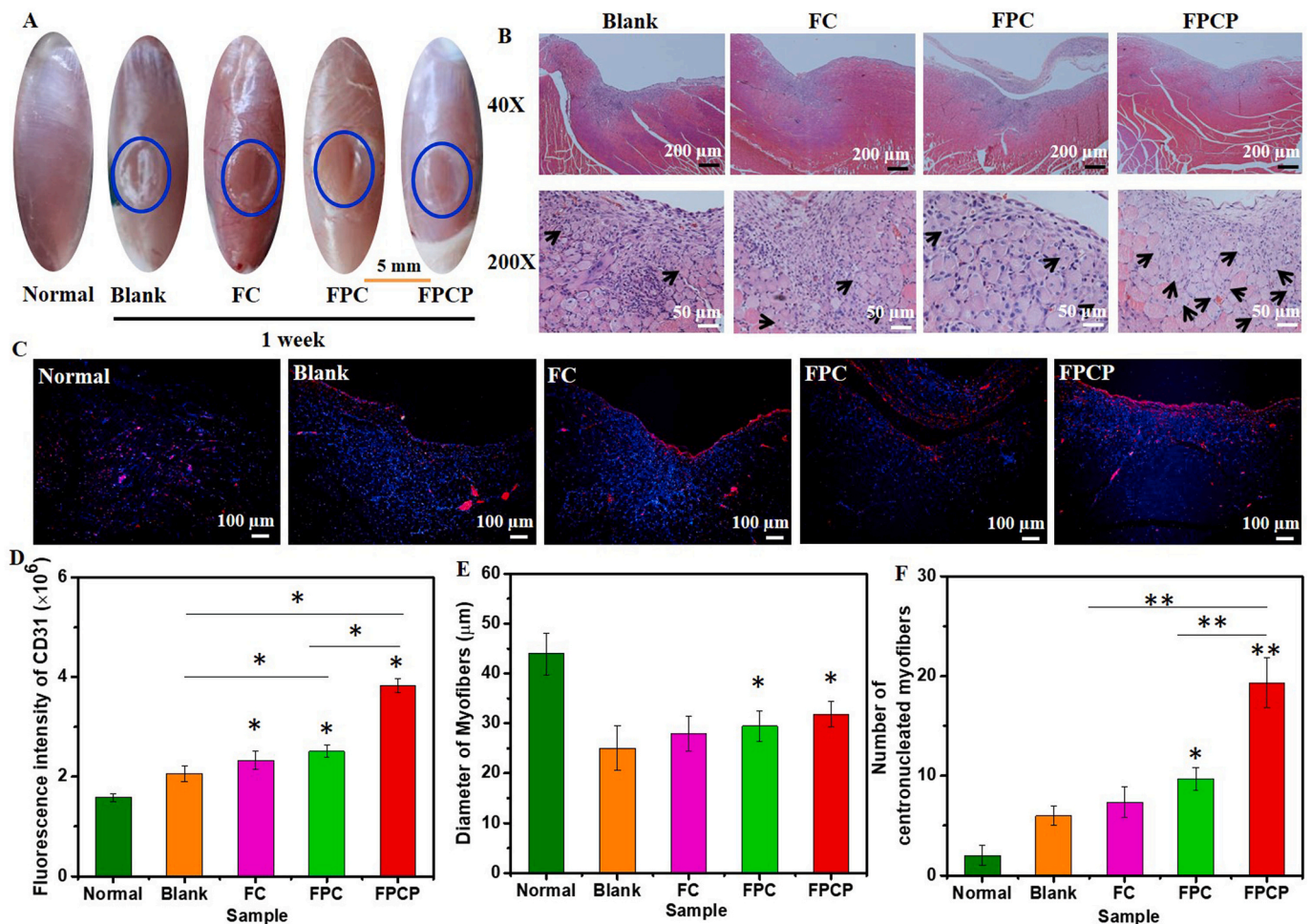
Fig. 7. Skeletal muscle regeneration *in vivo* after treated with FPCP hydrogel for 1 week (blue: sham operation). (A) Images of skeletal muscle defect; (B) H&E staining pictures of skeletal muscle defect area, the black arrows indicate the centronucleated myofibers; (C) CD 31 stained (red: CD 31, blue: nuclei) images; (D) quantitative analysis of CD 31, (E) Diameter of myofibers, and (F) numbers of regenerated myofibers (centronucleated myofibers) around the defect area in all groups. Three randomly selected fields of each section and three sections per specimen were analyzed by Image J software (*$p < 0.05$ and **$p < 0.01$).

could fit with the defect and efficiently scavenge free radicals located in the defect site, thereby decreasing the inflammation and promoting skeletal muscle repairing (Fig. 4D and E). Moreover, the higher electrical conductivity of FPCP could also accelerate the cell proliferation and myogenic differentiation of C2C12 cells by up-regulating the expressions of myogenic genes, which was beneficial to skeletal muscle regeneration *in vivo* (Figs. 4F and 6 and Fig. S5).

In this study, the as-prepared FPCP hydrogel showed intrinsically multifunctional properties including injectability, adhesive behavior, antioxidant and conductive activity, photothermo-responsive ability, which enabled the enhanced myoblast differentiation and skeletal muscle regeneration. Thus, FPCP hydrogel could fit and adhere to the muscle defect by smeared it on the defect sites during the minimally invasive surgery by comparison with traditional hydrogels or scaffolds [53,54]. FPCP hydrogel showed excellent photothermal performance, which could efficiently release protein under the control of NIR irradiation. It is probably speculated that the growth factors, genes or drugs loaded in FPCP hydrogel could be photo-controlled released, which was easier to control the release rate of them in FPCP hydrogel than other pH/redox-sensitive hydrogels [55]. Additionally, FPCP demonstrated better adhesive property, which could enhance the integration of the muscle tissue and hydrogel without the help of other adhesives [14,52]. The excellent antioxidant ability and conductive activity of FPCP hydrogel could enhance myoblast proliferation and muscle regeneration by decreasing the oxidative stress and reactive oxygen species and

enhancing angiogenesis which has important role in tissue regeneration [18]. The bioactive performance for FPCP in stimulating tissue formation was similar with previously reported bioactive biomaterials [56, 57]. Moreover, FPCP showed negligible cytotoxicity in C2C12 cells because of the better biocompatibility of each component. FPCP could achieve the purpose that enhanced skeletal muscle regeneration without the help of growth factors, stem cells or genes, which could simplify the experimental operation and reduce the cost [58]. This study suggests that FPCP hydrogel is a hopeful candidate for skeletal muscle regenerative medicine.

4. Conclusions

In summary, an injectable multifunctional bioactive nanomatrix was developed for enhancing myogenic differentiation and the full-thickness skeletal muscle regeneration *in vivo*. FPCP displayed strong shear-thinning behavior and good injectable ability, excellent photothermal performance under NIR irradiation, which could achieve the photo-controlled protein release. Importantly, FPCP possessed intrinsically multifunctional features including the adhesive property, antioxidant ability and electrical conductivity. FPCP hydrogel could enhance the cell proliferation and myogenic differentiation of C2C12 myoblasts by promoting the expressions of myogenic genes and MHC protein. FPCP hydrogel effectively promoted the full-thickness skeletal muscle regeneration *in vivo* through enhancing the myofiber formation and
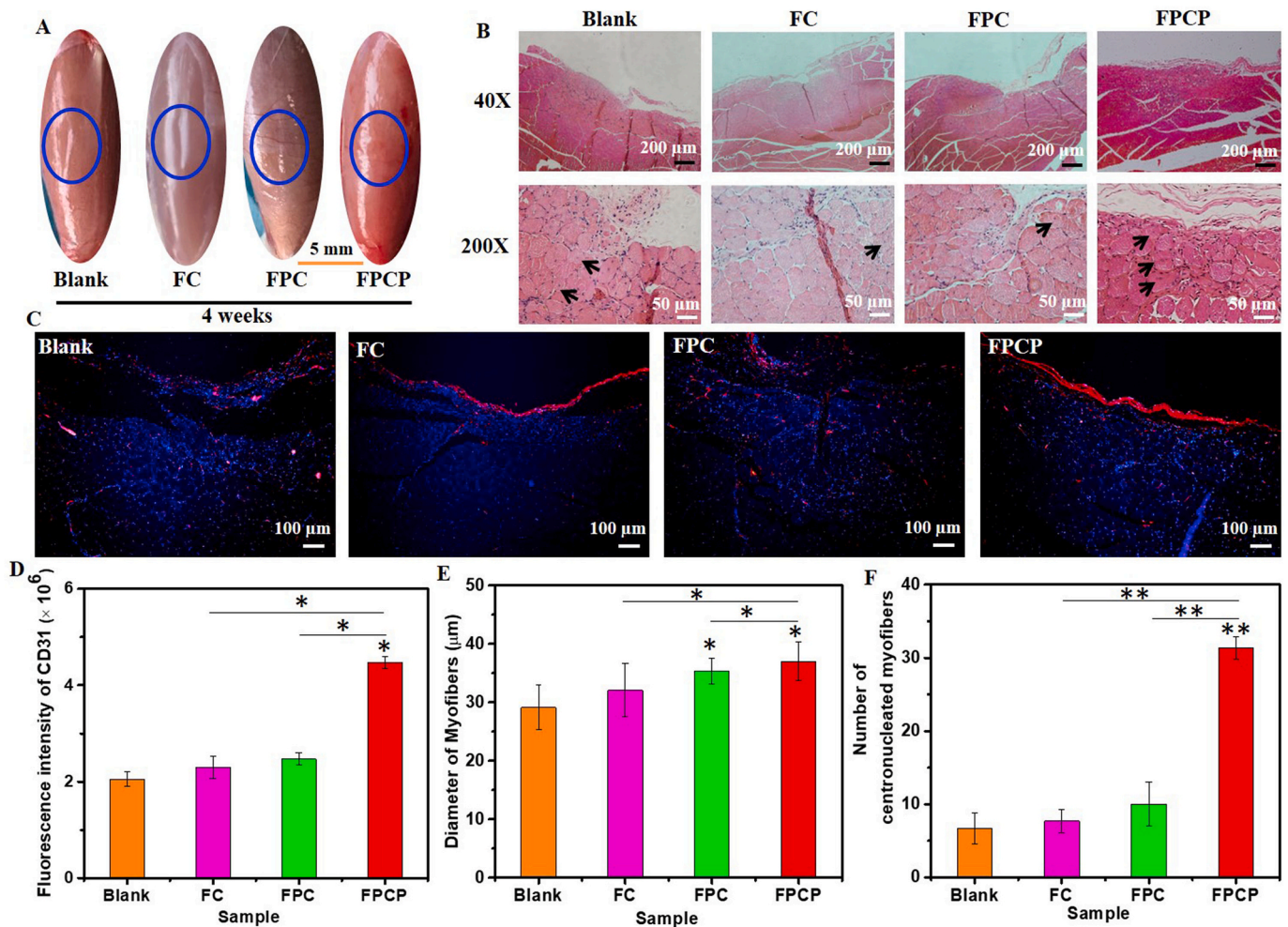
Fig. 8. Skeletal muscle regeneration *in vivo* after treated with FPCP hydrogel for 4 weeks (blue: sham operation). (A) Image of skeletal muscle defect; (B) H&E staining pictures of skeletal muscle defect area, the black arrows display centronucleated myofibers; (C) CD 31 stained (red: CD 31, blue: nuclei) images; (D) quantitative analysis of CD 31, (E) Diameter of myofibers, and (F) numbers of regenerated myofibers (centronucleated myofibers) around the defect area in all groups. Three randomly selected fields of each section and three sections per specimen were analyzed by Image J software (*$p < 0.05$ and **$p < 0.01$).

angiogenesis capacity. This study firstly indicated the vital role of multifunctional PPy@PDA nanoparticles in regulating myogenic differentiation and skeletal muscle regeneration. This work suggests that efficient tissue regeneration could be carried out by adjusting the structure and multifunctional features of biomaterials.

CRediT authorship contribution statement

Li Zhou: Formal analysis, Investigation, Validation, Writing - original draft. **Juan Ge:** Investigation, Writing - review & editing. **Min Wang:** Validation. **Mi Chen:** Investigation. **Wei Cheng:** Investigation, Validation. **Wenchen Ji:** Investigation, Validation. **Bo Lei:** Conceptualization, Writing - review & editing, Supervision.

Declaration of competing interest

The authors declare that they have no known competing financial interests or personal relationships that could have appeared to influence the work reported in this paper.

Acknowledgments

Appendix A. Supplementary data

Supplementary data to this article can be found online at https://doi.org/10.1016/j.bioactmat.2020.11.005.

References

[1] C.A. Cezar, D.J. Mooney, Biomaterial-based delivery for skeletal muscle repair, Adv. Drug Deliv. Rev. 84 (2015) 188–197, https://doi.org/10.1016/j.addr.2014.09.008.

[2] M. Juhas, N. Bursac, Engineering skeletal muscle repair, Curr. Opin. Biotechnol. 24 (2013) 880–886, https://doi.org/10.1016/j.copbio.2013.04.013.

[3] K.J. Gilmore, M. Kita, Y. Han, A. Gelmi, M.J. Higgins, S.E. Moulton, G.M. Clark, R. Kapsa, G.G. Wallace, Skeletal muscle cell proliferation and differentiation on polypyrrole substrates doped with extracellular matrix components, Biomaterials 30 (2009) 5292–5304, https://doi.org/10.1016/j.biomaterials.2009.06.059.

[4] L. Rao, Y. Qian, A. Khodabukus, T. Ribar, N. Bursac, Engineering human pluripotent stem cells into a functional skeletal muscle tissue, Nat. Commun. 9 (2018) 126, https://doi.org/10.1038/s41467-017-02636-4.

[5] B.L. Rodriguez, L.M. Larkin, Functional three-dimensional scaffolds for skeletal muscle tissue engineering. Functional 3D Tissue Engineering Scaffolds, 2018, pp. 279–304, https://doi.org/10.1016/B978-0-08-100979-6.00012-4.

[6] J. Ge, K. Liu, W. Niu, M. Chen, M. Wang, Y. Xue, C. Gao, P.X. Ma, B. Lei, Gold and gold-silver alloy nanoparticles enhance the myogenic differentiation of myoblasts through p38 MAPK signaling pathway and promote in vivo skeletal muscle regeneration, Biomaterials 175 (2018) 19–29, https://doi.org/10.1016/j.biomaterials.2018.05.027.

[7] B. Richard, N.J. Cassidy, S.H. Cartmell, Conductive polymers: towards a smart biomaterial for tissue engineering, Acta Biomater. 10 (2014) 2341–2353, https://doi.org/10.1016/j.actbio.2014.02.015.

[8] Y. Du, J. Ge, Y. Li, P.X. Ma, B. Lei, Biomimetic elastomeric, conductive and biodegradable polycitrate-based nanocomposites for guiding myogenic differentiation and skeletal muscle regeneration, Biomaterials 157 (2018) 40–50, https://doi.org/10.1016/j.biomaterials.2017.12.005.

[9] C. Ning, Z. Zhou, G. Tan, Y. Zhu, C. Mao, Electroactive polymers for tissue regeneration: developments and perspectives, Prog. Polym. Sci. 81 (2018) 144–162, https://doi.org/10.1016/j.progpolymsci.2018.01.001.

[10] T. Nezakati, A. Seifalian, A. Tan, A.M. Seifalian, Conductive polymers: opportunities and challenges in biomedical applications, Chem. Rev. 118 (2018) 6766–6843, https://doi.org/10.1021/acs.chemrev.6b00275.

[11] L. Han, L. Yan, M. Wang, K. Wang, L. Fang, J. Zhou, J. Fang, F. Ren, X. Lu, Transparent, adhesive, and conductive hydrogel for soft bioelectronics based on light-transmitting polydopamine-doped polypyrrole nanofibrils, Chem. Mater. 30 (2018) 5561–5572, https://doi.org/10.1021/acs.chemmater.8b01446.

[12] A.J. Hackett, J. Malmstrom, J. Travas-Sejdic, Functionalization of conducting polymers for biointerface applications, Prog. Polym. Sci. 70 (2017) 18–33, https://doi.org/10.1016/j.progpolymsci.2017.03.004.

[13] Y. Li, N. Li, G. Xue, W. Niu, M. Chen, Y. Du, P. Ma, B. Lei, Biodegradable thermal imaging-tracked ultralong nanowire-reinforced conductive nanocomposites elastomers with intrinsical efficient antibacterial and anticancer activity for enhanced biomedical application potential, Biomaterials 201 (2019) 68–76, https://doi.org/10.1016/j.biomaterials.2019.02.013.

[14] C. Xie, P. Li, H. Lu, Z. Wang, T. Zhou, W. Deng, K. Wang, L. Xiong, Electroresponsive and cell-affinitive polydopamine/polypyrrole composite microcapsules with a dual-function of on-demand drug delivery and cell stimulation for electrical therapy, NPG Asia Mater. 9 (2017) e358, https://doi.org/10.1038/am.2017.16.

[15] D. Gan, L. Han, M. Wang, W. Xing, T. Xu, H. Zhang, K. Wang, L. Fang, X. Lu, Conductive and tough hydrogels based on biopolymer molecular templates for controlling in situ formation of polypyrrole nanorods, ACS Appl. Mater. Interfaces 10 (2018) 36218–36228, https://doi.org/10.1021/acsami.8b10280.

[16] D. Browe, J. Freeman, Optimizing C2C12 myoblast differentiation using polycaprolactone–polypyrrole copolymer scaffolds, J. Biomed. Mater. Res. 107 (2019) 220–231, https://doi.org/10.1002/jbm.a.36556.

[17] J.Y. Lee, C.A. Bashur, A.S. Goldstein, C.E. Schmidt, Polypyrrole-coated electrospun PLGA nanofibers for neural tissue applications, Biomaterials 30 (2009) 4325–4335, https://doi.org/10.1016/j.biomaterials. 2009.04.042.

[18] Y. Zhu, Z. Cankova, M. Iwanaszko, S. Lichtor, M. Mrksich, G.A. Ameer, Potent laminin-inspired antioxidant regenerative dressing accelerates wound healing in diabetes, Proc. Natl. Acad. Sci. U.S.A. 115 (2018) 6816–6821, https://doi.org/10.1073/pnas.1804262115.

[19] M.E. Lynge, S. Philipp, S.D. Brigitte, Recent developments in poly(dopamine)-based coatings for biomedical applications, Nanomedicine 10 (2015) 2725–2742, https://doi.org/10.2217/nnm.15.89.

[20] L. Han, K. Liu, M. Wang, K. Wang, L. Fang, H. Chen, J. Zhou, X. Lu, Mussel-inspired adhesive and conductive hydrogel with long-lasting moisture and extreme temperature tolerance, Adv. Funct. Mater. 28 (2018) 1704195, https://doi.org/10.1002/adfm.201704195.

[21] H. Zhang, T. Zhao, B. Newland, W. Liu, W. Wang, W. Wang, Catechol functionalized hyperbranched polymers as biomedical materials, Prog. Polym. Sci. 78 (2018) 47–55, https://doi.org/10.1016/j.progpolymsci.2017.09.002.

[22] P. Zhou, F. Wu, T. Zhou, X. Cai, S. Zhang, X. Zhang, Q. Li, Y. Li, Y. Zheng, M. Wang, F. Lan, G. Pan, D. Pei, S. Wei, Simple and versatile synthetic polydopamine-based surface supports reprogramming of human somatic cells and long-term self-renewal of human pluripotent stem cells under defined conditions, Biomaterials 87 (2016) 1–17, https://doi.org/10.1016/j.biomaterials.2016.02.012.

[23] G. Pan, S. Sun, W. Zhang, R. Zhao, W. Cui, F. He, L. Huang, S.-H. Lee, K.J. Shea, Q. Shi, H. Yang, Biomimetic design of mussel-derived bioactive peptides for dual-functionalization of titanium-based biomaterials, J. Am. Chem. Soc. 138 (2016) 15078–15086, https://doi.org/10.1021/jacs.6b09770.

[24] J. Yang, A.R. Webb, G.A. Ameer, Novel citric acid-based biodegradable elastomers for tissue engineering, Adv. Mater. 16 (2004) 511–516, https://doi.org/10.1002/adma.200306264.

[25] B. Jiang, L. Perrin, D. Kats, T. Meade, G. Ameer, Enabling non-invasive assessment of an engineered endothelium on ePTFE vascular grafts without increasing oxidative stress, Biomaterials 69 (2015) 110–120, https://doi.org/10.1016/j.biomaterials.2015.07.064.

[26] M. Wang, M. Chen, W. Niu, D.D. Winston, W. Cheng, B. Lei, Injectable biodegradation-visual self-healing citrate hydrogel with high tissue penetration for microenvironment-responsive degradation and local tumor therapy, Biomaterials 261 (2020) 120301, https://doi.org/10.1016/j.biomaterials.2020.120301.

[27] L. Zhang, M. Wang, M. Chen, W. Niu, W. Liu, T. Leng, W. Ji, B. Lei, A safe and efficient bioactive citrate-lysine/miRNA33agonist nanosystem for high fat diet-induced obesity therapy, Chem. Eng. J. (2020) 127304, https://doi.org/10.1016/j.cej.2020.127304.

[28] Y. Xi, J. Ge, M. Wang, M. Chen, W. Niu, W. Cheng, Y. Xue, C. Lin, B. Lei, Bioactive anti-inflammatory, antibacterial, antioxidative silicon-based nanofibrous dressing enables cutaneous tumor photothermo-chemo therapy and infection-induced wound healing, ACS Nano 14 (2020) 2904–2916, https://doi.org/10.1021/acsnano.9b07173.

[29] W. Liu, M. Wang, W. Cheng, W. Niu, M. Chen, M. Luo, C. Xie, T. Leng, L. Zhang, B. Lei, Bioactive antiinflammatory antibacterial hemostatic citrate-based dressing with macrophage polarization regulation for accelerating wound healing and hair follicle neogenesis, Bioact. Mater. 6 (2020) 721–728, https://doi.org/10.1016/j.bioactmat.2020.09.008.

[30] M. Chen, F. Zhao, Y. Li, M. Wang, X. Chen, B. Lei, 3D-printed photoluminescent bioactive scaffolds with biomimetic elastomeric surface for enhanced bone tissue engineering, Mater. Sci. Eng. C 106 (2020) 110153, https://doi.org/10.1016/j.msec.2019.110153.

[31] B. Jiang, R. Suen, J.-J. Wang, Z.J. Zhang, J.A. Wertheim, G.A. Ameer, Vascular scaffolds with enhanced antioxidant activity inhibit graft calcification, Biomaterials 144 (2017) 166–175, https://doi.org/10.1016/j.biomaterials.2017.08.014.

[32] K.H. Nakayama, M. Shayan, N.F. Huang, Engineering biomimetic materials for skeletal muscle repair and regeneration, Adv. Healthcare Mater. 8 (2019), e1801168, https://doi.org/10.1002/adhm.201801168.

[33] T. Liu, X. Zhang, B. Ke, Y. Wang, X. Wu, G. Jiang, T. Wu, G. Nie, F-127-PEI co-delivering docetaxel and TFPI-2 plasmid for nasopharyngeal cancer therapy, Mater. Sci. Eng. C 61 (2016) 269–277, https://doi.org/10.1016/j.msec.2015.12.049.

[34] M. Wang, C. Wang, M. Chen, Y. Xi, W. Cheng, C. Mao, T. Xu, X. Zhang, C. Lin, W. Gao, Y. Guo, B. Lei, Efficient angiogenesis-based diabetic wound healing/skin reconstruction through bioactive antibacterial adhesive ultraviolet shielding nanodressing with exosome release, ACS Nano 13 (2019) 10279–10293, https://doi.org/10.1021/acsnano.9b03656.

[35] A. Serpen, E. Capuano, V. Fogliano, V. Gokmen, A new procedure to measure the antioxidant activity of insoluble food components, J. Agric. Food Chem. 55 (2007) 7676–7681, https://doi.org/10.1021/jf071291z.

[36] J. Hur, K. Im, S.W. Kim, J. Kim, D.-Y. Chung, T.-H. Kim, K.H. Jo, J.H. Hahn, Z. Bao, S. Hwang, N. Park, Polypyrrole/agarose-based electronically conductive and reversibly restorable hydrogel, ACS Nano 8 (2014) 10066–10076, https://doi.org/10.1021/nn502704g.

[37] D. Gan, T. Xu, W. Xing, X. Ge, L. Fang, K. Wang, F. Ren, X. Lu, Mussel-inspired contact-active antibacterial hydrogel with high cell affinity, toughness, and recoverability, Adv. Funct. Mater. 29 (2019) 1805964, https://doi.org/10.1002/adfm.201805964.

[38] F. Yu, X. Cao, J. Du, G. Wang, X. Chen, Multifunctional hydrogel with good structure integrity, self-healing, and tissue-adhesive property formed by combining diels-alder click reaction and acylhydrazone bond, ACS Appl. Mater. Interfaces 7 (2015) 24023–24031, https://doi.org/10.1021/acsami.5b06896.

[39] D. Gopinath, M.R. Ahmed, K. Gomathi, K. Chitra, P.K. Sehgal, R. Jayakumar, Dermal wound healing processes with curcumin incorporated collagen films, Biomaterials 25 (2004) 1911–1917, https://doi.org/10.1016/s0142-9612(03)00625-2.

[40] L. Zhou, Y. Xi, Y. Xue, M. Wang, Y. Liu, Y. Guo, B. Lei, Injectable self-healing antibacterial bioactive polypeptide-based hybrid nanosystems for efficiently treating multidrug resistant infection, skin-tumor therapy, and enhancing wound healing, Adv. Funct. Mater. 29 (2019) 1806883, https://doi.org/10.1002/adfm.201806883.

[41] J. Shao, C. Ruan, H. Xie, Z. Li, H. Wang, P.K. Chu, X.-F. Yu, Black-phosphorus-incorporated hydrogel as a sprayable and biodegradable photothermal platform for postsurgical treatment of cancer, Adv. Sci. 5 (2018) 1700848, https://doi.org/10.1002/advs.201700848.

[42] J. Li, C. Xie, J. Huang, Y. Jiang, Q. Miao, K. Pu, Semiconducting polymer nanoenzymes with photothermic activity for enhanced cancer therapy, Angew. Chem. Int. Ed. 57 (2018) 3995–3998, https://doi.org/10.1002/anie.201800511.

[43] J. Li, K. Pu, Development of organic semiconducting materials for deep-tissue optical imaging, phototherapy and photoactivation, Chem. Soc. Rev. 48 (2019) 38–71, https://doi.org/10.1039/c8cs00001h.

[44] Y. Jiang, P.K. Upputuri, C. Xie, Z. Zeng, A. Sharma, X. Zhen, J. Li, J. Huang, M. Pramanik, K. Pu, Metabolizable semiconducting polymer nanoparticles for second near-infrared photoacoustic imaging, Adv. Mater. 31 (2019) 1808166, https://doi.org/10.1002/adma.201808166.

[45] E.N. Zare, M.M. Lakouraj, M. Mohseni, Biodegradable polypyrrole/dextrin conductive nanocomposite: Synthesis, characterization, antioxidant and antibacterial activity, Synth. Met. 187 (2014) 9–16, https://doi.org/10.1016/j.synthmet.2013.09.045.

[46] M. Shi, M. Ishikawa, N. Kamei, T. Nakasa, N. Adachi, M. Deie, T. Asahara, M. Ochi, Acceleration of skeletal muscle regeneration in a rat skeletal muscle injury model by local injection of human peripheral blood-derived CD133-positive cells, Stem Cell. 27 (2010) 949–960, https://doi.org/10.1002/stem.4.

[47] K. Sadtler, K. Estrellas, B.W. Allen, M.T. Wolf, H. Fan, A.J. Tam, C.H. Patel, B. S. Luber, H. Wang, K.R. Wagner, Developing a pro-regenerative biomaterial scaffold microenvironment requires T helper 2 cells, Science 352 (2016) 366–370, https://doi.org/10.1126/science.aad9272.

[48] A.S. Hoffman, Stimuli-responsive polymers: biomedical applications and challenges for clinical translation, Adv. Drug Deliv. Rev. 65 (2013) 10–16, https://doi.org/10.1016/j.addr.2012.11.004.

[49] M. Wang, Y. Guo, Y. Xue, W. Niu, M. Chen, P.X. Ma, B. Lei, Engineering multifunctional bioactive citric acid-based nanovectors for intrinsical targeted tumor imaging and specific siRNA gene delivery in vitro/in vivo, Biomaterials 199 (2019) 10–21, https://doi.org/10.1016/j.biomaterials.2019.01.045.

[50] M.C.G. Pella, M.K. Lima-Tenorio, E.T. Tenorio-Neto, M.R. Guilherme, E.C. Muniz, A.F. Rubira, Chitosan-based hydrogels: from preparation to biomedical applications, Carbohydr. Polym. 196 (2018) 233–245, https://doi.org/10.1016/j.carbpol.2018.05.033.

[51] Y. Guo, M. Wang, J. Ge, W. Niu, M. Chen, W. Cheng, B. Lei, Bioactive biodegradable polycitrate nanoclusters enhances the myoblast differentiation and in vivo skeletal muscle regeneration via p38 MAPK signaling pathway, Bioact. Mater. 5 (2020) 486–495, https://doi.org/10.1016/j.bioactmat.2020.04.004.

[52] R. Balu, S. Reeder, R. Knott, J. Mata, L. de Campo, N.K. Dutta, N.R. Choudhury, Tough photocrosslinked silk fibroin/graphene oxide nanocomposite hydrogels, Langmuir 34 (2018) 9238–9251, https://doi.org/10.1021/acs.langmuir.8b01141.

[53] M.F. de Jesus Raposo, A.M. Bernardo de Morais, R.M. Santos Costa de Morais, Marine polysaccharides from algae with potential biomedical applications, Mar. Drugs 13 (2015) 2967–3028, https://doi.org/10.3390/md13052967.

[54] R. Chen, J. Wang, C. Liu, Biomaterials act as enhancers of growth factors in bone regeneration, Adv. Funct. Mater. 26 (2016) 8810–8823, https://doi.org/10.1002/adfm.201603197.

[55] L. Chen, X. Yao, Z. Gu, K. Zheng, C. Zhao, W. Lei, Q. Rong, L. Lin, J. Wang, L. Jiang, M. Liu, Covalent tethering of photo-responsive superficial layers on hydrogel surfaces for photo-controlled release, Chem. Sci. 8 (2017) 2010–2016, https://doi.org/10.1039/c6sc04634g.

[56] M. Yu, Y. Du, Y. Han, Lin, B. Lei, Biomimetic elastomeric bioactive siloxane-based hybrid nanofibrous scaffolds with miRNA activation: a joint physico-chemical-biological strategy for promoting bone regeneration, Adv. Funct. Mater. 30 (2020) 1906013, https://doi.org/10.1002/adfm.201906013.

[57] Y. Xue, W. Niu, M. Wang, M. Chen, Y. Guo, B. Lei, Engineering a biodegradable multifunctional antibacterial bioactive nanosystem for enhancing tumor photothermo-chemotherapy and bone regeneration, ACS Nano 14 (2020) 442–453, https://doi.org/10.1021/acsnano.9b06145.

[58] E. Ruvinov, S. Cohen, Alginate biomaterial for the treatment of myocardial infarction: progress, translational strategies, and clinical outlook from ocean algae to patient bedside, Adv. Drug Deliv. Rev. 96 (2016) 54–76, https://doi.org/10.1016/j.addr.2015.04.021.